Articles

# Climate and Smoke: An Appraisal of Nuclear Winter

R. P. TURCO, O. B. TOON, T. P. ACKERMAN, J. B. POLLACK, C. SAGAN

**The latest understanding of nuclear winter is reviewed. Considerable progress has been made in quantifying the production and injection of soot by large-scale fires, the regional and global atmospheric dispersion of the soot, and the resulting physical, environmental, and climatic perturbations. New information has been obtained from laboratory studies, field experiments, and numerical modeling on a variety of scales (plume, mesoscale, and global). For the most likely soot injections from a full-scale nuclear exchange, three-dimensional climate simulations yield midsummer land temperature decreases that average 10° to 20°C in northern mid-latitudes, with local cooling as large as 35°C, and subfreezing summer temperatures in some regions. Anomalous atmospheric circulations caused by solar heating of soot is found to stabilize the upper atmosphere against overturning, thus increasing the soot lifetime, and to accelerate interhemispheric transport, leading to persistent effects in the Southern Hemisphere. Serious new environmental problems associated with soot injection have been identified, including disruption of monsoon precipitation and severe depletion of the stratospheric ozone layer in the Northern Hemisphere. The basic physics of nuclear winter has been reaffirmed through several authoritative international technical assessments and numerous individual scientific investigations. Remaining areas of uncertainty and research priorities are discussed in view of the latest findings.**

CRUTZEN AND BIRKS (*1*) RECOGNIZED THAT SMOKE GENERated in a nuclear exchange might affect the transmission of sunlight through the atmosphere over most of the Northern Hemisphere and thus perturb weather patterns significantly. Turco *et al.* (*2*) advanced the scientific analysis in three broad areas: quantification of key parameters describing smoke and dust production and physical properties; identification of the basic physical processes underlying and initiated by large-scale smoke injections; and estimation of the atmospheric and climatic impacts of nuclear war–generated smoke and dust. Turco *et al.* projected average land surface coolings in the range of 10° to 25°C, maximum continental-interior land surface coolings in the range of 30° to 35°C, and extensive regions of prolonged freezing—the nuclear winter effect. These calculations, which assumed annual average solar conditions and separately treated land and ocean surfaces, were offered as first-order estimates of the potential global-scale impacts of multiple nuclear detonations.

Subsequent in-depth scientific assessments that have focused on the nuclear winter problem include studies by the U.S. National Academy of Sciences (*3*), the International Council of Scientific Unions (*4, 5*), and the World Meteorological Organization (*6*). Dozens of scientific articles and reviews have been published on the subject (*7*), and the U.S. Office of Science and Technology Policy has organized a national program to study nuclear winter. All of these analyses, including the most recent update by the Scientific Committee on Problems of the Environment (SCOPE) (*8*) and a scientific report from the United Nations (*9*), have concluded that the widespread environmental effects of nuclear war could threaten most of the human population (*10–12*). Although any prediction of the aftermath of a nuclear conflict remains uncertain (*13*), intensive research during the last 5 years has markedly improved our understanding of the basic physical underpinning of the nuclear winter theory.

Recent investigations (*6, 8, 9*) have reached the following general conclusions: (i) sufficient smoke could be generated during nuclear warfare to decrease average solar intensities by 50% or more on a hemispheric scale; (ii) sooty smoke from urban fires is the major contributor to nuclear winter; (iii) average land cooling beneath the smoke clouds could reach 10° to 20°C and continental interiors could cool by up to 20° to 40°C with subzero temperatures possible even in summer; (iv) upper air layers could be heated by as much as 100°C; (v) smoke heated in this manner would be stabilized against removal by convective penetration; and (vi) interhemispheric transport and horizontal mixing of the smoke clouds would be greatly accelerated by the heating. In addition, the original prediction (*2*) that intermediate time-scale radioactive fallout would be greater by an order of magnitude than previous estimates is now generally accepted (*4, 8*).

Over the past 5 years, many significant refinements have been made to the original nuclear winter theory. However, as one might expect, adjustments of the large number of parameters that affect nuclear winter have been offsetting to a large degree. Hence, as the science has matured, relatively minor changes have occurred in predicted effects. Moreover, new phenomena have been discovered that exacerbate the environmental impacts, including severe ozone depletion in the Northern Hemisphere. In this article, we summarize the research that has developed since 1983 and present new estimates of smoke emissions and optical effects.

R. P. Turco is at the University of California, Los Angeles, CA 90024. O. B. Toon and J. B. Pollack are at the NASA Ames Research Center, Moffett Field, CA 94035. T. P. Ackerman is at Pennsylvania State University, University Park, PA 16802. C. Sagan is at Cornell University, Ithaca, NY 14853.

## Flammables

The quantities of flammable materials in urban areas have been discussed in a number of reports (*2–4, 14*). The data, collected in Table 1, are based primarily on production rather than end use, although end use urban fuel-loading estimates are consistent with these values (*14*). The principal categories of fuels considered in nuclear winter studies are lumber and other man-made cellulosic materials, petroleum and fossil carbon–based fuels, plastics and related synthetics, asphalt and similar compounds, and vegetation.

Lumber is a principal construction material. We estimate that about 9000 teragrams (Tg = $10^{12}$ g) of sawn (or milled) wood is contained in existing structures worldwide (*15*), neglecting raw timber used in construction, fencing, and so forth. This value is between lower (6,300 Tg) (*16*) and higher (12,600 Tg) estimates (*4, 17*).

Two-thirds of global petroleum refining capacity is concentrated at as few as 200 sites, and the quantities of crude petroleum and products in primary storage are reasonably well established (Fig. 1). Data developed for the United States show an inventory of about 180 Tg, including about 50 Tg in the underground "strategic reserve" (*16*). Extrapolated to the entire developed world, these figures imply total primary stocks of about 730 Tg (Table 1). Common Market data have been analyzed independently to estimate about 800 Tg of primary stores worldwide (*4, 17*), including up to 100 Tg on ships in port and transit. Secondary petroleum stocks in smaller storage reservoirs are more uncertain; estimates range from 100 to 700 Tg (*4, 16, 17*). Asphalt used in roofing, and thus highly vulnerable to fire, amounts to 400 Tg worldwide (Table 1).

At the present time, about 400 to 500 Tg of plastics are in use in the developed world (Table 1). When burned, plastics generate a variety of toxic gases, including hydrogen chloride and hydrogen cyanide, that are environmentally hazardous (*2–4*). The current plastics inventory is expected to double early in the next century (*18*). Up to 3000 Tg of plastics could exist at refuse sites by that time (*18*), although most of this would be unlikely to burn in a nuclear exchange.

Many additional flammables likely to be ignited in a general nuclear conflict, such as coal and natural gas, urban and rural vegetation (*19, 20*), foodstuffs, tar insulation, petrochemicals, lubricating oils, paints, and finishes (*2, 4, 17*), are not explicitly accounted for in the present fuel inventory. These materials might add roughly 10% to the total fuel burden (except in particular cases such as coal stores, which are comparable in mass to petroleum stocks).

The most recent inventories of flammables are one-half to one-third the earliest estimates (*1–3*) in certain categories, such as construction lumber. However, the inventory estimates for oil, plastics, and related compounds have remained stable (Table 1). The overall uncertainty in the combustible loading is probably now less than ~50%; specific sources of uncertainty are discussed in the references cited in Table 1.

## Ignition Scenarios

The nuclear arsenals of the United States and the Soviet Union now hold about 25,000 strategic warheads carrying roughly 10,000 megatons (MT = $1 \times 10^{15}$ cal = 1000 kT) of explosive energy (*21*). Because an average 400-kT airburst is capable of burning an area of up to 300 to 500 km$^2$ (*3, 4*), the existing arsenals have the potential to cause enormous damage through fire, aside from their other lethal effects. Roughly 50% of the total U.S. urbanized area (~75,000 km$^2$, including open spaces), in addition to vast rural areas of farmland and natural vegetation (~500,000 km$^2$), would be subject to intense incendiary effects in some nuclear war scenarios, and up to ~1500 Tg of flammables would be affected [in the absence of fire spread (*14*)]. Accordingly, for a nuclear exchange in which key military and industrial sites are extensively targeted, collateral fire ignition is expected to consume 25 to 75% of the available urban flammable materials (in the combatant nations). Almost all of this fuel would be consumed in active flaming combustion (*4, 14*).

If cities were intentionally targeted, rather than being collateral targets as assumed above, an aggregate of only ~100 MT (~1% of the arsenal yield) in ~100-kT nuclear warheads would be capable of igniting up to one-half of the available urban flammables concentrated in the major commercial and industrial centers (*22*). Petroleum storage and refining facilities are considered to be primary strategic

**Table 1.** Inventory of flammables. All masses are given in teragrams (Tg = $1 \times 10^{12}$ g). The total masses reflect the minimum, maximum, and average (of the minimum and maximum) fuel inventory figures. The vegetation inventories for the developed world are the same as for NATO and Warsaw Pact nations. Other potential fuels are not included in the total (*1–4*).

| Materials | NATO and Warsaw Pact (Tg) | Developed world (Tg) | Reference |
|---|---|---|---|
| Wood and lumber* | 5,500<br>11,000<br>7,800 | 6,300†<br>12,600‡<br>9,000§ | (*16*)<br>(*4, 17*)<br>(*15*) |
| Primary petroleum products | 480<br>530¶ | 730†‖<br>800 | (*16*)<br>(*4, 17*) |
| Secondary petroleum | 100<br>200–460¶ | 150†¶<br>300–700 | (*16*)<br>(*4, 17*) |
| Plastics and polymers | 343<br>400‖<br>400** | 400†‖<br>460<br>460‖ | (*16*)<br>(*4, 17*)<br>(*18*) |
| Asphalt roofing | 335<br>170¶ | 500†¶<br>250 | (*16*)<br>(*4, 17*) |
| Vegetation†† | 150<br>750 | | (*19*)<br>(*20*) |
| Total | 6,740–13,480<br>(10,100) | 7,980–15,810<br>(11,900) | |

*Construction lumber produced as sawnwood, not including plywood and certain other wood products. †Bing's estimated inventories for all cellulosic materials in the United States and the NATO and Warsaw Pact nations are ~2100 Tg and ~6400 Tg, respectively. The latter figure can be scaled upward by a factor of 1.15 [see Penner (*13*)] to obtain an estimate of ~7400 Tg of cellulosics for the developed world. Of this total, we estimate that about 85% is lumber (in residential and nonresidential buildings); 10% is plywood, pressboard, and paneling; and 5% is paper, cardboard, and fabrics. Thus, Bing's analysis yields about 1800 Tg of lumber in the United States, 5500 Tg in the NATO and Warsaw Pact nations, and 6300 Tg in the developed world. For petroleum, Bing estimates primary reserves of about 480 Tg in the NATO and Warsaw Pact countries, from which the world primary stocks may be estimated as ~730 Tg [see footnote ‖]. Similarly, Bing's NATO and Warsaw Pact value for plastics of 343 Tg may be scaled upward to ~400 Tg. For asphalt roofing, Bing finds 335 Tg in the NATO and Warsaw Pact nations, which we increase to ~500 Tg for the entire developed world [see footnote ¶]. Likewise for secondary petroleum stocks, which are scaled from 100 Tg to 150 Tg worldwide. ‡For the developed world, the total mass of cellulosics is estimated to be about 15,000 Tg, of which 1000 Tg is paper, cardboard, and related products. Of the 14,000 Tg of wood and building materials, about 90%, or 12,600 Tg, would be lumber and related products. §The United States produces about 45 Tg of sawnwood annually, the Soviet Union about 55 Tg per year, and all nations about 225 Tg. The figures are derived from the annual volume of sawnwood (*15*) with an average density of 0.5 g/cm$^3$ for cured lumber. The "lifetime" for lumber in U.S. structures is roughly 40 years [with a total U.S. construction lumber inventory of 1800 Tg (*16*) divided by a production rate of 45 Tg per year]. This lifetime implies an accumulated global mass of lumber of 9000 Tg. Production of roundwood (*15*), much of which is used as fuel, is roughly four times that of sawnwood worldwide. ‖Estimated assuming that 87% of the total in the developed world is held in the NATO and Warsaw Pact nations [see Penner (*13*)]. ¶Estimated assuming that 66% of the total is held in the NATO and Warsaw Pact nations (*16*). **Plastics production in Japan is assumed to contribute to the NATO and Warsaw Pact inventories. ††Vegetation that is subject to ignition near isolated military targets such as missile fields.

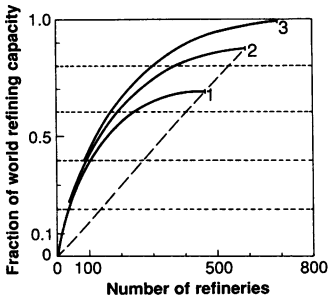


**Fig. 1.** Fraction of the world petroleum refining capacity versus the cumulative number of refineries. Data on refinery capacity are from (*131*). Curves are given for three groupings of countries: (1) The United States and NATO allies, the U.S.S.R. and Eastern Bloc nations, and China; (2) The countries of group 1 plus the Middle East, Japan, Australia, and several other nations closely aligned with the superpowers; (3) All nations with significant refining capacity. For each grouping, the individual refineries are ordered by refining capacity, with the largest first. A random summation of refinery capacities would correspond to the dashed line (for groups 1 and 2). Petroleum storage is correlated with refining capacity (*131*). Storage sites away from refineries are also highly concentrated (*23, 132*). Liquid fuel storage tanks are extremely vulnerable to nuclear detonations; a tactical explosion of 10 kT could destroy tankage over an area of up to 15 $km^2$ (*133*).

targets (*21, 23*). Because of their concentration and vulnerability, as few as several megatons carried by several hundred tactical-yield nuclear warheads would be capable of destroying most of the world's primary petroleum stocks (*24*) (Fig. 1).

In the original studies (*1–3*), specific targets such as oil refineries were mentioned, but not carefully enumerated. Instead, total areas of general urban destruction were estimated; those areas are roughly comparable to the most recent estimates discussed above (*14*).

## Emission Factors

Smoke produced in combustion has a variety of forms. Smoldering combustion generates light-colored smoke consisting of oily droplets composed of low-volatility organic compounds. Flaming combustion produces black sooty smoke. Electron microscopy reveals that soot particles are formed as chain aggregates of very small solid spherules that have a low H:C ratio and the characteristic signature of graphite under x-ray diffractometry (*25*). The soot aggregates coagulate to form clusters containing thousands of spherules with an open morphology of low fractal order [~2 (*26*)], which is important in determining the soot optical properties (*27, 28*). The fractal order is maintained as the aggregates continue to grow by coagulation, unless the soot is exposed to high humidity.

In large fires, the smoke will consist of a number of components including oily droplets, soot aggregates, mixed oil and soot particles, windblown dust and debris, flying ash, and background (ambient) aerosols. However, from the point of view of optical and climatic consequences, the soot component is the most critical because of its high light-absorption efficiency (*29*). Accordingly, in this article emphasis is placed on soot produced by flaming combustion (*30*).

The mass of soot generated per unit mass of fuel burned is defined as the soot-emission factor. The yield of soot depends on the material burned and the conditions of combustion. Typically, soot-emission factors are high for plastics and heavy petroleum products and are lower for wood and other cellulosic compounds. The soot-emission factor also tends to increase as fire size is increased and as ventilation (that is, oxygen supply) is restricted (*31*).

Most data on soot emissions from common urban fuels has been obtained in small- and medium-scale laboratory test fires (*1–4, 29, 32–35*). For plastics, soot yields can range from a few percent to more than 10%. Considering the mix of plastics currently in use (*18*) and recent emission-factor measurements, an average emission factor for plastics of 5% would seem to be conservative, with 10% equally likely in building fires. In the case of petroleum and fuel products, the limited data from laboratory experiments (*32*) and a few open pool fires (*36*) indicate that emission factors of 3 to 10% are applicable at the scales appropriate to nuclear war (*32, 36*).

Wood and vegetation are the most abundant combustible materials. Free-burning vegetation appears to have a very slow soot-emission factor of about 0.1% to 0.3% (*35, 37*). Small, well-ventilated wood crib fires emit up to 0.4% soot (*32, 33*). However, experiments with larger wood cribs (~100 kg) and partially restricted ventilation have yielded emission factors of up to 3% (*33*). These results may apply to large-scale urban fires, in which the burning conditions in steel and concrete structures are likely to involve restricted air flow. Accordingly, an average soot-emission factor of 1% for wood is chosen to represent the conditions in urban conflagrations; the range of possible emission factors is between about 0.2% and 3%.

In our earlier study (*2*), an average smoke-emission factor for mixed urban fuels was estimated to be ~4% (~2% in central city firestorms) and for vegetation, ~3%. Ten to 20% of the smoke was presumed to consist of soot, with an average soot-emission factor of about 0.5%—roughly five to six times smaller than the mean value in Table 2.

## Prompt Scavenging

Soot particles can be immediately scavenged and removed (*38*) from large fire plumes as "black rain," which is induced by the strong buoyant convection and condensation of moisture (*2–4*). The extent of soot removal depends on the amount of fire-induced rain and the efficiency with which soot particles are incorporated into water droplets and ice crystals that subsequently coalesce and fall out as precipitation (*4, 39*). Under reasonable physical assumptions, detailed computer simulations of cloud processes indicate that particle collection by Brownian diffusion, phoretic accretion, and gravitational impaction would scavenge at most a few percent of the soot particles emitted into convective fire plumes (*40*). Electrical charging might influence the soot scavenging rate (*41*), but no quantitative estimates of this effect are available.

Fresh soot particles are hydrophobic and, therefore, will be relatively poor cloud condensation nuclei (CCN) (*42*). Laboratory studies of the CCN activity of a variety of smokes supports this idea; whereas ~25 to 75% of wood smoke particles participate as CCN at 1% supersaturation, only about 1% of kerosene soot particles are active as CCN (*43*), even after "aging" in holding bags for 30 min. These CCN fractions are not significantly larger after 5 hours of aging. The laboratory results for wood smoke are consistent with extensive data collected in a series of large-scale field burns (*43*). The measured concentrations of CCN in the vegetation fire columns ranged from $10^5$ to $10^6$ $cm^{-3}$, which exceeds ambient CCN concentrations by two to three orders of magnitude.

The low CCN activity of soot particles generated from certain liquid organic fuels (kerosene, for instance) has been confirmed by direct measurements of CCN abundances in large pool fire plumes (*43*). Even though the total particle concentrations exceeded $10^4$ $cm^{-3}$ in these experiments, the CCN concentrations remained indistinguishable from ambient levels (that is, $\leq$1000 $cm^{-3}$). A similar result was obtained earlier in a soot plume generated by burning heavy diesel fuel (*43*). However, there is some evidence that soot produced from crude petroleum may have greater CCN activity (*44*).

In a fire plume, numerous particles in addition to soot would be present to act as CCN. These include background tropospheric aerosols (~100 to 1000 $cm^{-3}$) (*45*), windblown dust and ash (*41*),

and oily smoke particles ($10^3$ to $10^5$ $cm^{-3}$) (*46*). These CCN would compete with soot for the limited condensible water vapor available in the plume. If more than $\sim 10^3$ cloud droplets are nucleated per cubic centimeter of air, then the small resulting cloud droplet sizes inhibit coalescence and formation of precipitation (*41, 47*). Simulations of strong updrafts in which smoke CCN concentrations are as high as $\sim 10^5$ $cm^{-3}$ show very low precipitation efficiencies (*48*) and overall prompt smoke removal fractions of only ~0.1 of the nucleated smoke particles (*40, 49, 50*).

The overall prompt scavenging of soot (the most climatically active component of the smoke) is limited by several factors. First, soot particles initially are relatively ineffective CCN (*51*); hence, only a small fraction (~10% of the total mass) is likely to be directly scavenged by nucleation (and phoretic processes) in the condensation zone of a fire plume (*52*). The fraction subsequently removed by precipitation would be less than 10%, unless other scavenging processes contributed significantly. Further, the "overseeding" of fire-capping clouds by high CCN concentrations could inhibit precipitation, further restricting the soot removal.

Originally, we (*2*) estimated that 25 to 50% of the smoke mass would be immediately scrubbed from urban fires by induced precipitation. However, based on current data, it is more reasonable to assume that, on average, ≤10 to 25% of the soot emission is likely to be removed in such a manner. This conclusion, which allows for some removal of soot, is consistent with the occasional observation of "black rains" at large historical fires (*2–4*).

## Injection Heights

The height of smoke injection above a fire depends on the fire size, intensity and duration, and the local meteorological state of the atmosphere. Hydrodynamical simulations of city-size fires predict that smoke would be injected into the middle and upper troposphere, with some direct injection (perhaps 10% of the smoke) into the lower stratosphere (*40, 53, 54*). Even relatively small fires inject smoke above the atmospheric boundary layer (*37*), whereas large forest conflagrations deposit smoke in the vicinity of the tropopause (*55*). Subsequent heating and lofting of the smoke over a period of days following injection is discussed below.

Several smoke-injection profiles have been recommended or used to make climate predictions for massive smoke injections associated with a nuclear war (Fig. 2). The smoke-injection heights vary over a substantial range, with the lowest injection profile having a mass centroid at 2.8 km (*56*), and the highest at 6.5 km. A new study of smoke injection, in which detailed estimates of fuel loadings and rates of combustion were used to force a convective plume model, suggests smoke injection centroids in the range of 4 to 6 km (*14, 54*), consistent with our original estimates (*2*).

## Water Injection

Water is also injected with smoke in large fire plumes. The water is responsible for prompt scavenging and could produce persistent clouds, which would affect subsequent rainout and create radiative anomalies (*3*). On a hemispheric scale, the amount of water likely to be injected with smoke could perturb background water vapor concentrations by at most a few percent (*3*), because the mass of water involved is relatively small (*57*). Although in many cases the injected water, which had escaped depletion by precipitation, would initially be supersaturated and therefore predominantly condensed into clouds, the dilution and warming of the smoky air would tend to dissipate the condensation within days (*58*).

## Smoke Optics

Considerable interest has focused on the absorption of light by soot (*59*), the variation of absorption with smoke composition and morphology, and the change in absorption with physical and chemical aging of the smoke aerosol. Also of importance is the wavelength dependence of these properties. For the present purposes, it is adequate to consider the soot optical coefficients at two

**Table 2.** Potential soot absorption optical depths averaged over the Northern Hemisphere (*59*). The most likely parameter values are based on the discussion in the text; a range is also given for each parameter and for the corresponding optical depth. The absorption coefficient for soot is taken to be 7 $m^2/g$ (range of 4 to 10 $m^2/g$), and the prompt soot removal efficiency is taken to be 20% (range of 10 to 25%). For a discussion of uncertainties see (*91*).

| Flammable material | Quantity burned* (Tg) | Soot emission factor | Soot emission (Tg) | Absorption optical depth |
|---|---|---|---|---|
| Wood and lumber | 4000 (2000–6000) | 0.01 (0.002–0.02) | 40 (4–120) | 0.88 (0.05–4.3) |
| Primary petroleum | 400 (200–600) | 0.06 (0.03–0.10) | 24 (6–60) | 0.54 (0.07–2.2) |
| Secondary petroleum | 200 (50–500) | 0.06 (0.03–0.10) | 12 (1.5–50) | 0.27 (0.02–1.8) |
| Plastic and polymers | 200 (100–300) | 0.08 (0.05–0.10) | 16 (5–30) | 0.36 (0.06–1.1) |
| Asphalt roofing | 125 (60–200) | 0.10 (0.06–0.13) | 12.5 (3.6–26) | 0.28 (0.04–0.9) |
| Vegetation | 150 (150–750) | 0.003 (0.001–0.005) | 0.45 (0.15–3.8) | 0.010 (0.002–0.14) |
| Total | 5075 (2560–8350) | | 105 (20–290) | 2.3 (0.24–10.4) |

*For wood, plastics, and asphalt roofing, roughly 50% of the NATO and Warsaw Pact inventories from Table 1 is assumed to burn in flaming combustion (range of 25 to 75%). For the primary petroleum stocks, about 50% of the total world inventory (or 80% of the NATO and Warsaw Pact inventory) is assumed to be highly vulnerable to ignition in a nuclear war (range of 25 to 75% of the world inventory). In the case of the secondary petroleum stocks, ~50% of the average NATO and Warsaw Pact inventory is assumed to burn; the lower value is one-half of the smallest inventory estimate (*16*) and the upper value is 75% of the largest inventory estimate (*17*). For vegetation, the lower fuel estimate of Small and Bush (*19*) is adopted, with a range spanning the current estimates (*19, 20*).

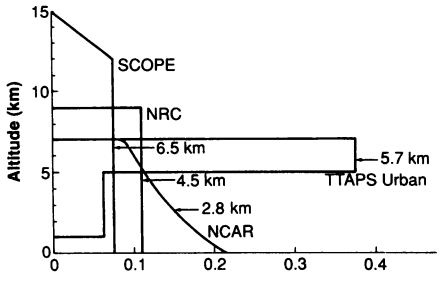


**Fig. 2.** Smoke injection profiles for nuclear winter smoke and climate studies. The profiles are normalized to a "unit" smoke injection, expressed as a fractional smoke mass per kilometer of altitude. The altitude above and below which half the smoke was inserted (that is, the smoke mass centroid) is indicated (arrows) for each profile. The NCAR profile corresponds to injections between 0 and 7 km with a uniform "mixing ratio" (*56*). The TTAPS (*2*) and NRC (*3*) profiles are discussed in those reports and have been used in the past for nuclear winter simulations. The SCOPE injection profile has been recommended (*8*) for urban fires based on data and simulations of large-scale fire plumes (*3, 4, 8*).

wavelengths: mid-visible (~550 nm) and thermal, or long-wave, infrared (~10 μm). In order to determine the optical absorption contributed by a given fuel, the inventory, emission factor, and specific absorptivity must be combined (*59*).

A large number of measurements on various soots at visible wavelengths yield specific absorptivities (*59*) that range from low value of 3 to 4 $m^2/g$ to high values of 10 to 12 $m^2/g$ (*32, 34, 35, 60–63*). However, when the data are normalized against the elemental carbon (EC) content of the soot, the range of specific absorptivities is about 6 to 11 $m^2$ per gram of EC. For the sources of soot relevant to atmospheric problems, a median absorptivity of ~7 $m^2$ per gram of soot is appropriate at 550-nm wavelength. That the specific absorptivity of soot is relatively independent of the particle source (or size distribution) is consistent with the theory of light absorption by soot-like fractal aggregates (*27, 28*).

The specific absorptivity of soot is expected to decrease as the particle aggregate size increases, if the aggregates become more compact with size. Investigations on carbon black reveal a significant reduction in tinting strength when the primary (fused) aggregate size exceeds an equivalent spherical diameter of about 0.4 μm (*64*). Preliminary laboratory studies indicate that the decrease in soot absorptivity owing to coagulation might be as large as 30% (*63*), with final specific absorptivities still ≥6 $m^2/g$. The applicability of these results under atmospheric conditions must still be determined.

The condensation of moisture or fuel vapors on soot clusters can affect the morphology of the particles and hence their optical and physical properties (*65*). New laboratory studies of soot aggregates generated by aging, dense, sooty smoke for up to 16 hours shows that exposure to supersaturations of ≤3% causes only small variations in optical properties (*32, 63*). Even large soot aggregates exposed to very high supersaturations of 90 to 130% show a negligible decrease in specific absorptivity (from 6.9 to 6.7 $m^2/g$) (*32*) and a moderate decrease in overall light extinction power (by 23 to 45% for soots aged over periods of 0.5 to 4 hours) (*63*).

When soot is mixed with nonabsorbing materials (for example, oils or ammonium sulfate), the absorptivity generally remains in the range 6 to 11 $m^2$ per gram of EC (*60, 62, 66*). With dilute mixtures of soot in water, or with soot as a surfactant on water droplets, the soot absorbing power (per unit mass) may actually increase by 10 to 100% (*67*).

The spectral dependence of light extinction (*59*) by sooty smoke was recently measured from ~0.35 to 2.5 μm in a large kerosene pool fire plume (*68*). The extinction fell off slowly with increasing wavelength, unlike the behavior for fresh vegetation smoke in this spectral region (*68*). By implication, soot is a strong absorber (*59*) throughout the solar spectrum.

At long infrared wavelengths, the absorption (and extinction) coefficient of soot is lower than at visible wavelengths (*69*). Extrapolation of the pool fire data (*68*) in accordance with expected behavior (*69*), plus independent data from $CO_2$ laser propagation measurements on soot (*61, 70*), indicate that the absorptivity in the visible is about ten times that in the thermal infrared (*71*). A direct comparison of the absorption in acetylene soot at wavelengths of 515 nm and 10.6 μm shows a ratio ~11 (*61*). New laboratory measurements of "urban" smoke properties suggest that the factor could be as large as ~30 (*34, 72*). [Another study of soot from diesel fuel found that the absorption coefficient at a wavelength of 10 μm was ~0.8 $m^2/g$ (and the extinction coefficient, ~1.0 $m^2/g$) whether or not large soot aggregates were present (*70*).]

The original nuclear winter climate studies (*2, 3*) assumed an average visible absorptivity of about 1.5 to 2 $m^2/g$ for mixtures of sooty and oily smokes. That assumption is consistent with the observed strong absorption of light by soot when mixtures made up of 10 to 20% soot by mass are assumed (*2*). In the long-wave infrared spectrum, no significant revisions have had to be made to the smoke optical properties since the early work.

## Aging and Reaction

The aging of soot particles can alter their optical and physical properties. Coagulation generates larger particles, which could have a smaller specific absorptivity [as Mie theory predicts (*64, 73*)] if the fractal order of the aggregates increases (*27, 28*). Highly agglomerated (*63*) and compacted (*64*) soots exhibit this behavior to some degree. Collection by soot particles of sulfates and other nonabsorbing materials should not affect the absorbing power of the soot substantially (*66, 67*), but would leave the soot particles more vulnerable to precipitation scavenging.

Photochemical aging of soot can occur by accretion of inorganic compounds (such as sulfates) and by decomposition. For example, graphite and carbon black are known to react with ozone (*74, 75*), which is plentiful in the upper atmosphere. New laboratory investigations show, however, that the reaction is too slow, even under the most favorable conditions, to reduce the chemical lifetime of soot particles below 1 to 2 years (*75*). Accordingly, the residence time and removal of war-generated soot clouds would be controlled by dynamical and microphysical processes (*2*).

Over the long term, the removal of tropospheric soot by precipitation would be fairly efficient. In one field experiment, a soot washout ratio (that is, the soot concentration in rainwater relative to that in the local airmass) of $4.8 \times 10^5$ was determined for urban-generated soot (*76*). Typical washout ratios for sulfates range from $4 \times 10^5$ to $80 \times 10^5$ (*77*). Under ambient conditions, the soot is usually a minor component associated with the background hygroscopic (largely sulfate) aerosol (*78, 79*). However, in situations where soot has been recently released into the atmosphere, its washout efficiency is found to be considerably lower than for the background aerosol (*76*). Apparently the soot does not mix "internally" with the ambient aerosols on short time scales (hours to days).

In our original work (*2*), smoke aging by coagulation was explicitly treated (*73*); however, chemical reactions that might deplete soot were ignored, which is consistent with the latest laboratory results.

## Regional Dispersion

The regional (or mesoscale) dispersion of large smoke plumes has been investigated through mathematical simulation (*80–82*), wildfire plume sampling (*37*), and historical data analysis (*83*). During

the first few days of smoke dispersion, particle coagulation and washout may be significant. Our capability for simulating the regional behavior of large aerosol plumes has greatly improved in recent years (*81, 82*). Model calculations coupled with satellite photography show that smoke is transported within days over hemispheric distances (*84*) and that as much as a third of the smoke may be washed out in frontal systems during the first few days, if the smoke particles are assumed to be good CCN (*81*).

Regional-scale smoke plumes generated by large forest fires have been observed to cause surface temperature decreases of several degrees Centigrade (*85, 86*). Wildfires in Alberta, Canada, in 1982 were responsible for reducing the average daytime surface temperatures in the north-central United States by 1.5° to 4°C (*83*). More recently, the massive Chinese wildfires of May 1987 were found to reduce daytime temperatures over Alaska by 2° to 6°C (*83*). In September 1987, a series of large wildfires erupted in southern Oregon and northern California. During one period, a dense smoke pall covered the Klamath River valley for 3 weeks. Recorded daytime temperatures were as much as 20°C below normal values (*83*). In all of these instances, the minimum nighttime temperatures were not significantly affected. The magnitude of the daytime cooling is consistent with theoretical expectations for the surface temperature effects of forest fire smoke [given its specific optical properties (*35*)] (*2, 87*).

Natural dust clouds provide another means of studying aerosol dispersion, coagulation, removal, and radiative transfer (*81, 88*). Dust is also produced in large quantities by surface and near surface nuclear detonations and is directly relevant to the nuclear winter problem (*89*). Typically, surface cooling of several degrees centigrade or more is observed beneath dense windblown dust clouds (*88*).

Smoke from urban fires, which is much more absorbing than smoke from wildfires and is generally injected higher in the atmosphere, would produce even stronger surface cooling effects (*2, 87*). Solar heating of sooty smoke clouds during the first few days would also lead to enhanced lofting of the smoke and accelerated mesoscale dispersion (*80–82, 90*).

The earliest nuclear winter assessments (*2, 3*), which relied on observations of dust storms and large-scale wildfire plumes for guidance, assumed that multiple smoke and dust clouds generated by a nuclear war would be widely dispersed over the Northern Hemisphere within 1 to 2 weeks (*2*). This is consistent with our present understanding, although the actual distributions would be patchy rather than uniform.

## Optical Depths

In order to investigate the potential effects of smoke emissions on global climate, the optical depths of widespread smoke clouds must be estimated. The absorption optical depth (*59*) at visible wavelengths (specifically, at 550 nm) is the most useful parameter and is calculated here with the assumption that the injected smoke is uniformly distributed over the Northern Hemisphere.

The data in Table 2 suggest that hemispheric average absorption optical depths of ~2 to 3 could occur (*91*) in a full-scale nuclear exchange [involving the North Atlantic Treaty Organization (NATO) and Warsaw Pact nations]. Even the lowest optical depth in Table 2, ~0.24, implies a potential average hemispheric reduction in insolation of about 35% (*92*). Concerted nuclear attacks against urban and industrial centers at relatively low aggregate yield (~100 MT) are capable of producing smoke palls with average optical depths ≥1 (see section on Ignition Scenarios). Attacks against oil refineries, at even lower megatonnage (*24*), could still generate average absorption optical depths of ~1.

The estimated smoke emissions and optical depths are sensitive to the detonation scenario, which of course cannot be accurately predicted. However, a wide range of nuclear exchange scenarios could lead to the conditions described in Table 2 (*3, 4, 21*).

The latest SCOPE smoke-injection scenarios (*8*) define a range of equivalent hemispheric absorption optical depths of 0.3 to 3.0; no probability is attached to these values and they may be considered as equally probable (*93*). The SCOPE optical depth range falls within that defined in Table 2.

During the initial period of smoke emission to the atmosphere after a nuclear exchange—before the smoke had spread to hemispheric scales (that is, in the first week or two of the conflict)—local optical depths would be patchy, with values both much larger and much smaller than the hemispheric average. At these times, it could be very dark beneath the smoke clouds, with severe depressions of surface temperatures (*82, 83*). However, the formation of ground fogs could moderate surface cooling by releasing latent heat and trapping surface infrared energy. The latent heat effect is generally explicitly accounted for in the climate model studies cited later in this article. The infrared trapping effect, which is not usually treated, can delay for a time, but cannot prevent, the surface cooling.

In earlier work (*2, 3*), the hemispheric average smoke absorption optical depths were roughly 1.4; the optical depth attributable to urban smoke alone was about 1.1 (*2*). These values are about half the total absorption optical depths in Table 2.

## Climate Impacts

Comprehensive modeling studies have been carried out to determine the effects of large smoke emissions on surface and atmospheric temperatures, circulation patterns, and precipitation and insolation. The models used for this work have, in many cases, been upgraded from standard climate models through improvements such as treatment of smoke as a radiatively active tracer, with infrared effects; interactive dynamical coupling of smoke heating and transport; inclusion of soil heat storage and transport, with modified surface air stability parameterization; and explicit resolution of diurnal variability. The physics used in various nuclear winter simulations are summarized in Fig. 3.

*Acute phase (first 1 to 3 months).* It is now well understood that extended smoke layers cool the underlying land surfaces (*2–4, 8, 9*). With absorption optical depths ≥0.5, the most important forcing mechanism is the reduction of solar heating at the surface, without sufficient compensating infrared heat transfer (*94*) from the atmosphere (*2, 4, 87*). With small absorption optical depths ($<<1$), slight warming is predicted for tropospheric soot residing near the surface, as in the case of Arctic haze (*95*). This situation is likely to develop only very late in the sequence of events following a nuclear war and is not large enough to be important. However, if the soot were to settle onto the northern snowpack, the surface energy balance could be perturbed significantly (*96–98*).

Predictions for land surface temperature changes are summarized in Fig. 3 (*2, 17, 56, 82, 87, 99–117*). The most severe perturbations occur primarily in the Northern Hemisphere mid-latitudes and subtropics. In the latest three-dimensional general circulation model (GCM) simulations, July smoke injections cause land temperatures averaged over the latitude zone from 30° to 70°N (and over a 5-day period) to decrease by ~5°C in the case of small smoke injections (optical depth ~0.3), ~13°C in the central SCOPE (*8*) smoke-injection case (absorption optical depth ~1), and ~22°C in the greater smoke-injection case (optical depth ~3). Maximal 24-hour average temperature drops within continental interiors reach 30° to

35°C or more with $\tau \geq 1$, and widespread frosts and freezing events can occur throughout the midlatitudes within the first month.

The temperature perturbations for smoke injections in other seasons are smaller. In winter, with solar insolation already limited, smoke-induced coolings of only several degrees are predicted. For spring smoke injections, the temperature decreases are only marginally smaller than for summer injections. However, because the land is cooler initially, the probability of frosts and freezing events is much higher.

At lower latitudes, the cooling is also moderated by several factors, including the delayed transport of smoke to these regions and the warmer and more humid climates at these latitudes. Nevertheless, GCM forecasts suggest coolings of 10°C or more with $\tau \geq 1$, particularly in the subtropical latitudes in the Northern Hemisphere. With the larger smoke injections (absorption optical depths ~3), extensive freezing can extend into the subtropics. The predicted temperature depressions, even with smaller smoke injections, imply potential massive crop losses both in low-latitude and mid-latitude regions (*5, 10*).

Calculated changes in precipitation during the acute phase are dramatic. The average decrease in rainfall over land in July at latitudes from 30° to 70°N, ~75% (*114*) is roughly constant for a wide range of optical depths (~0.3 to 3). For latitudes from 0° to 20°N, the reductions in precipitation range from about 25% at low optical depths to ~60 to 75% in cases where the most smoke would be produced (*114*). In most of the model simulations, failure of the summer Asian monsoon is forecast.

The reductions in light levels during the first weeks and months are also significant. The average decreases in solar insolation over land from 30° to 70°N latitude are ~40% with low amounts of smoke and ~90% with high amounts of smoke (*114, 115*). At low latitudes (0° to 20°N), the corresponding average light reductions are ~0 to 50%, respectively.

Remarkably, all of the climate analyses carried out over the last 5 years predict strong cooling beneath extended smoke clouds (with absorption optical depths of ~1) for a wide range of modeling assumptions about smoke-injection heights and washout rates and for different treatments of boundary layer and radiative effects (Fig. 3). The climatological perturbations induced within a matter of days to weeks after a major nuclear exchange would be unprecedented in human history. The predicted land temperature decreases (averaged over coastal and inland regions, for the coldest week-long period) differ by less than 50% between models when differences in smoke parameter assumptions (Fig. 3) are taken into account. Further, in

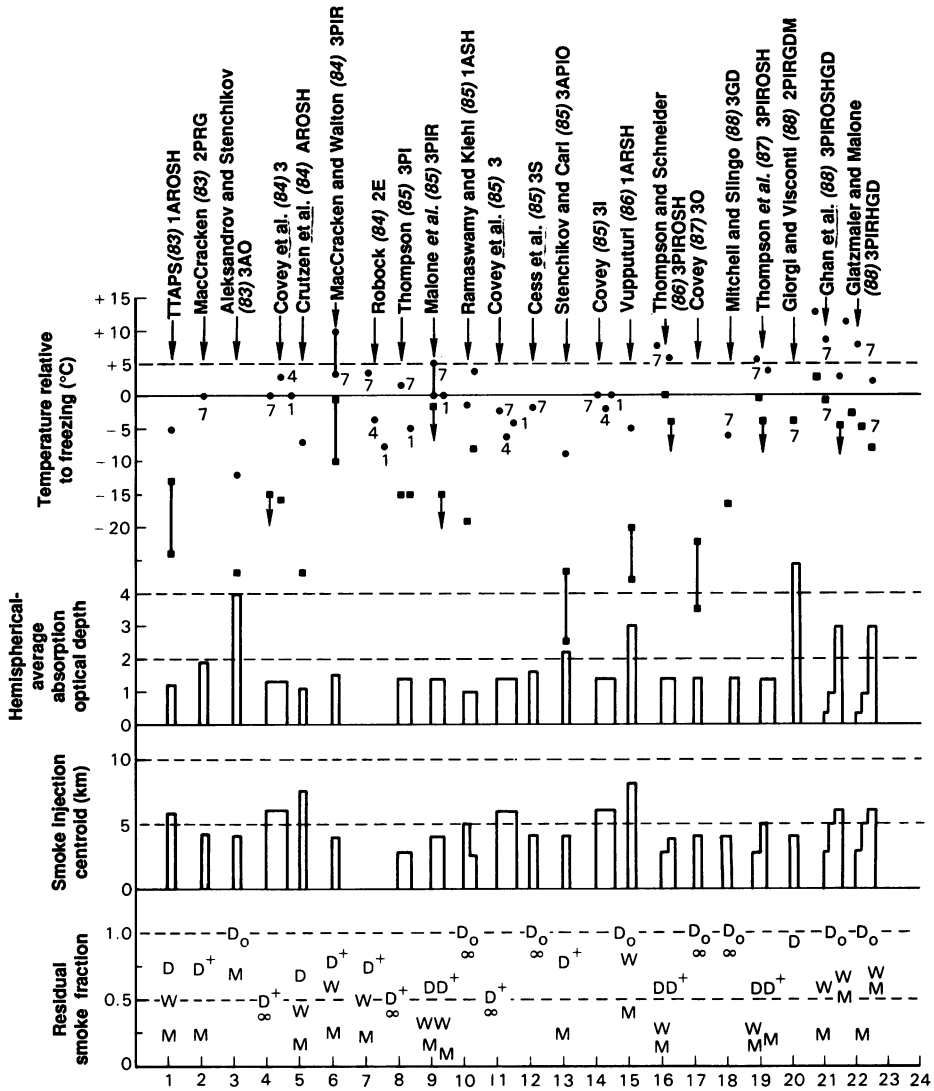


**Fig. 3.** Summary of nuclear winter climate model calculations. Data are shown for the following: (i) (●) Average land temperatures (coastal plus inland) in regions beneath widespread smoke layers for the coldest 1- to 2-week period in the simulation (some of the references report only temperature changes; the absolute temperatures have been deduced by subtracting the computed average temperature decrease from the temperature offset given below for each season); the month of the simulation is indicated by a numeral; for the 1-D radiative and convective models, the average land temperature decreases are taken as one-half of the "all-land" temperature decreases to account for the effect of ocean moderation (*2*); annual average solar insolation also applies in these cases. (ii) (■) Minimum land temperatures beneath smoke during the acute phase of nuclear winter simulations (again, where necessary, absolute temperatures were obtained by subtracting decreases from offsets); these temperatures are averaged over at least 1 day. (iii) Hemispheric average absorption optical depth of the smoke injection. (iv) Height centroid of the smoke mass injection. (v) Residual smoke fractions at several times in each simulation. [Data have been obtained from (*2, 17, 56, 82, 87,* and *99–115*) and certain data (missing from the figure) were not available.] The selected calculations roughly correspond to recommended "baseline" smoke injection scenarios (*3, 4, 8*); less severe and more severe cases have been investigated, but not as frequently as baseline cases. The studies have been ordered from left to right roughly in chronological sequence and are numbered along the bottom of the figure. For a given study, several cases may be illustrated (for example, the Ramaswamy and Kiehl (*87*) results are shown for two smoke-injection profiles]. The data are organized vertically for each simulation. The temperature offset used: 0°C, winter; 13°C annual, fall, and spring; 25°C, summer; and 35°C for cases calculated by Lawrence Livermore National Laboratories. The model treatments: 1, 2, and 3 indicate dimensions; A, annual solar insolation; P, patchy smoke injection; I, interactive transport; R, removal by precipitation; O, optical properties evolve; S, scattering included; H, infrared-active smoke; E, energy balance; G, ground heat capacity; D, diurnal variation; and M, mesoscale (48 hours). Smoke removal: D, after 1 day (prompt removal): $D_o$, arbitrary initial injection; W, after 1 week; M, after 1 month; $^+$, assumption implicit in smoke scenario adopted; and ∞, no smoke removal after injection.

most of the baseline simulations, land temperatures drop below freezing even in midsummer, although the extent and duration of these freezing events vary considerably.

*Chronic phase (first 1 to 3 years).* The original nuclear winter theory predicted that widespread smoke layers would be heated and stabilized against removal and that solar heating would drive smoke into the Southern Hemisphere at a rapid rate (*2*). These proposals were based on observations of analogous phenomena in nature (*118*) and on physical reasoning. Both predictions have been confirmed by more comprehensive model calculations (*90, 105*). The effects are important because smoke stabilization would determine the course of the long-term climatic impacts of a nuclear war, whereas interhemispheric transport would potentially spread effects to all nations (*4, 8, 9*).

Simulations for July smoke injections (*112, 114, 115*) indicate that 25 to 40% of the initial smoke injection would be stabilized against removal by precipitation with low-altitude injection [National Center for Atmospheric Research (NCAR) profile in Fig. 2] and up to 60% with higher injection (SCOPE profile in Fig. 2). The atmospheric residence time of the residual smoke is calculated to be ~1 year in these simulations. Moreover, after only 3 weeks the smoke is predicted to spread over the entire Northern Hemisphere and most of the Southern Hemisphere (from initial patches of injection over North America, Europe, and Western Asia). The global average absorption optical depth of the residual smoke layer can range up to ~0.5, which is sufficient to cause major energy balance perturbations (*119, 120*).

Long-term climate responses are difficult to predict because of the complex role of coupled energy feedback mechanisms that are not yet well represented in global climate models (*121*). A number of studies have focused on specific processes such as changes in the albedo of snow and ice fields caused by soot fall (*96–98*). These calculations indicate that substantial global temperature anomalies (several degrees or more) can appear in the postwar climatology. A few long-term (~1 year) simulations have been carried out by using GCMs with simplified smoke physics or lower spatial resolution (*111, 114, 116, 122*). On these time scales, the response of the ocean surface layer is critical, although the model representations of ocean processes are crude. Ocean surface temperature decreases of 2° to 6°C have been predicted; in combination with ice feedback effects, significant climatic cooling could therefore be expected during the second postwar summer (*103*).

Of considerable interest are the potential climatic perturbations in the Southern Hemisphere after a massive smoke injection at northern mid-latitudes. Clearly, the climate effects would be greatly attenuated from those in the Northern Hemisphere. Chronic nuclear winter calculations for Australia (*117, 120*) indicate average land temperature decreases of 2° to 4°C, sea surface temperature depressions of 2° to 3°C, reductions in precipitation by ~50%, and decreases in solar insolation and day length by 20 to 30% in the summer season. These effects would be expected to limit significantly agricultural productivity (*5*).

## Ozone Depletion

New simulations of perturbations to the stratospheric ozone layer caused by massive injections of smoke and nitrogen oxides ($NO_x$) suggest that long-term (several years) global ozone depletions of 50% or more are possible (*123*). The calculations—carried out by applying GCMs with interactive smoke and ozone transport, and including reactions of $NO_x$—show that the heated nuclear smoke pall, rising into the Northern Hemisphere stratosphere, physically displaces the ambient ozone layer toward the Southern Hemisphere. The $NO_x$ intermingled with the smoke photochemically erodes the remaining ozone. The fact that the smoke-laden air is heated by as much as 100°C in the model accelerates ozone destruction (*110*). Twenty days after a baseline soot injection (*4, 8*), the ozone layer in the Northern Hemisphere is reduced on average by 40 to 50%. Roughly half of this depletion is due to ozone displacement and half to chemical decomposition (*123*). On regional scales, the ozone depletions are even greater.

The nuclear winter ozone hole would lead to enhancements of biologically harmful ultraviolet (UV-B) solar radiation doses (by 100 to 200% or more above normal) at middle latitudes for a year or longer after the smoke had cleared [see (*124*) for a discussion of the UV-B dependence on ozone amount and (*125*) for a review of the biological effects of ultraviolet radiation]. The ozone depletion could grow worse beyond the first month (*1–4*), although long-term ozone simulations have yet to be carried out. The fate of the excess ozone pushed into the Southern Hemisphere stratosphere must also be determined.

## Uncertainties and Recommendations

The uncertainties in calculations of the climate effects of smoke emissions have been discussed at length in a number of reports (*3, 4, 13*), and specific uncertainties have been mentioned in this article. Nevertheless, as in any complex geophysical problem, there is no reliable quantitative methodology for determining the overall uncertainty in existing climate forecasts for nuclear winter. The uncertainty in the climate response to large smoke injections has been narrowed substantially since the first accounts in 1982 and 1983 (*1, 2*). Putting aside the uncertainty in fire-ignition scenarios, which can never be fully resolved (*126*), the existing data strongly suggest that significant global-scale climatic disturbances should be expected after a major nuclear exchange (*9*). In addition to the climatic anomalies that have been emphasized here, hazardous conditions would be caused by widespread malnutrition (*5*), radioactive fallout (*4, 127*), chemotoxic agents (*4, 128*), the breakdown of health and civil infrastructure supporting human survival (*11, 12*), and synergisms among these stresses.

The principal climatic parameters and processes requiring further definition include: (i) the initial scavenging and removal efficiency of soot by induced precipitation in large fire plumes; (ii) the net emission factors and optical absorption coefficients of soot released in massive convective firestorms; (iii) the dispersion of dense smoke and water clouds over regional scales and the effects of interactions with synoptic weather systems; (iv) the detailed surface energy response to persistent, widespread smoke layers, including the influence of fog formation, vegetative cover, and diurnal forcing; (v) the long-term (months to years) global climate anomalies caused by residual smoke and the geophysical feedback mechanisms that might be activated; (vi) the role of dust lofted by nuclear explosions in producing short- and long-term atmospheric optical anomalies and climatic effects; and (vii) the development and duration of global stratospheric ozone depletions—a hemisphere-wide nuclear winter ozone hole—and attendant ultraviolet radiation intensification.

There are other important effects concurrent with climate change that should be addressed because they bear on the overall environmental and societal impacts of nuclear war: (i) the dynamics of fire ignition and spread in natural and urban fuel arrays; (ii) chemical perturbations, including emissions of toxic compounds, remobilization of air pollutants (*129*), and widespread contamination of water, air, and soil; (iii) radioactive fallout, both prompt and delayed, local and global, from weapons detonations and from damaged military and civilian nuclear facilities and radioactive waste storage sites, with

exposures over short and long terms (*4, 127*); (iv) the response of agricultural systems (and other key ecosystems) to the combined effects of changes in temperature, insolation, precipitation, ultraviolet radiation, and other physical and environmental factors (*5, 10*); and (v) the impact of disruptions in medical, governmental, economic, and other societal systems on postconflict stress, survival, and recovery (*11, 12*).

## Conclusion

Our knowledge of the sources and climatic impact of soot in a nuclear war has advanced considerably since the early work on this subject (*1, 2*). The constellation of physical effects—attenuation of sunlight, surface cooling, upper-level heating and stabilization, and enhanced interhemispheric transport—proposed in the original nuclear winter hypothesis (*2*) have been reaffirmed through increasingly sophisticated theoretical and experimental analyses. Specific physical parameters have undergone substantial revision, but these adjustments have been mutually compensating and have not led to changes exceeding a factor of 2 in the magnitude of predicted effects (*130*). Although important uncertainties persist and more work remains to be carried out, the basic physics of nuclear winter appear to be firmly established. With regard to the long-term, widespread consequences of nuclear war, the existing data indicate that, should substantial urban areas or fuel stocks be exposed to nuclear ignition, severe environmental anomalies—possibly leading to more human casualties globally than the direct effects of nuclear war (*5, 8, 10*)—would be not just a remote possibility, but a likely outcome.

### REFERENCES AND NOTES


1. P. J. Crutzen and J. W. Birks, *Ambio* **11**, 114 (1982).
2. R. P. Turco, O. B. Toon, T. P. Ackerman, J. B. Pollack, C. Sagan, *Science* **222**, 1283 (1983); "Global Atmospheric Consequences of Nuclear War," report U122878 (R&D Associates, Marina del Rey, CA, March 1983); *Eos* **63**, 1018 (1982). From the names of the authors, these reports have been given the acronym TTAPS. Some 50 different cases were studied, thereby covering a plausible range of nuclear war scenarios and uncertain physical parameters.
3. National Research Council, *The Effects on the Atmosphere of a Major Nuclear Exchange* (National Academy of Sciences, Washington, DC, 1985).
4. A. B. Pittock *et al.*, *Environmental Consequences of Nuclear War*, vol. 1, *Physical and Atmospheric Effects* (SCOPE-28, Wiley, Chichester, England, 1986).
5. M. A. Harwell and T. C. Hutchinson, *Environmental Consequences of Nuclear War*, vol. 2, *Ecological and Agricultural Effects* (SCOPE-28, Wiley, Chichester, England, 1985).
6. G. S. Golitsyn and M. C. MacCracken, "Atmospheric and climatic consequences of a major nuclear war: Results of recent research", WCP-142 (World Meteorological Organization, Geneva, 1987); G. S. Golitsyn and N. A. Phillips, *World Meteorological Organization Report WCP-113* (February 1986).
7. L. A. McIntosh, "Select Bibliography on Nuclear Winter," *Pacific Sierra Research Corp. Note 743* (Los Angeles, CA, March 1987).
8. F. Warner *et al.*, *Environment* **30** (no. 5), 2 (1988); F. Warner *et al.*, *ibid.* **29**, 4 (1987).
9. "Study on the Climatic and Other Effects of Nuclear War", *United Nations Report A/43/351* (May 1988).
10. The biological implications of nuclear winter described in (*5*)—and most importantly the impacts on agriculture—have been independently assessed, and found to be in all likelihood underestimated [Committee on Interagency Radiation Research and Policy Coordination of the U.S. Office of Science and Technology Policy, *Science Panel Report #5 (ORAU 88/B-85)* (March 1988)].
11. World Health Organization, "Effects of Nuclear War on Health and Health Services," Geneva (1988).
12. *Medical Implications of Nuclear War*, F. Solomon and R. Q. Marston, Eds. (National Academy Press, Washington, DC, 1986).
13. B. G. Levi and T. Rothman, *Phys. Today* **38**, 58 (September 1985); A. A. Broyles, *Am. J. Phys.* **53**, 323 (1985); J. Penner, *Nature* **324**, 222 (1986); I. Colbeck and R. M. Harrison, *Atmos. Env.* **20**, 1673 (1986); A. Berger, *Eos* **67**, 617 (1986); S. H. Schneider and S. L. Thompson, *Nature* **333**, 221 (1988).
14. R. D. Small, B. W. Bush, M. A. Dore, *Aerosol Sci. Tech.* **10**, 37 (1989). Fuel loadings are assessed for U.S. urban areas by using detailed land-use data and surveys of urban combustible burdens. Potential smoke production is based on unclassified Department of Defense target lists used for vulnerability and damage assessments.
15. *Statistical Yearbook, 1979/80* (United Nations, New York, 1981).
16. G. Bing, "Estimates of total combustible material in NATO and Warsaw Pact Countries," *Lawerence Livermore National Laboratory Report UCRL-93192* (Livermore, CA, 1985).
17. P. J. Crutzen, I. E. Galbally, C. Brühl, *Clim. Change* **6**, 323 (1984).
18. R. P. Turco, in (*12*), p. 96.
19. R. D. Small and B. W. Bush, *Science* **229**, 465 (1985); B. W. Bush and R. D. Small, "Smoke produced by nonurban target-area fires following a nuclear exchange," *Defense Nuclear Agency Report DNA-TR-85-293-A* (Washington, DC, 1985).
20. T. P. Ackerman, J. M. Stenback, R. P. Turco, and H. D. Grover, unpublished calculations.
21. W. M. Arkin and R. W. Fieldhouse, *Nuclear Battlefields* (Ballinger, Cambridge, MA, 1985); T. B. Cochran, W. M. Arkin, M. M. Hoenig, *Nuclear Weapons Databook* (Ballinger, Cambridge, MA, 1984), vol. 1; *ibid.*, vol. 2 (1987). There are in addition some 30,000 tactical and theater nuclear warheads deployed, carrying a total yield of several hundred megatons.
22. The fact that cities are effectively on the strategic targeting lists of the superpowers is discussed in a number of reports [for example, R. Siegel, *Strategic Targetting Options* (MIT Press, Cambridge, MA, 1981)].
23. M. A. Sastry, J. J. Romm, K. Tsipis, "Nuclear crash: The U.S. economy after small nuclear attacks," *Program in Science and Technology for International Security, Report 17* (Massachusetts Institute of Technology, Cambridge, MA, 1987).
24. According to the data in Fig. 1, about two-thirds of the world petroleum refining capacity could be destroyed by ~200 warheads of ~1- to 10-kT yield targeted on sites in the warring nations and their allies, for an aggregate yield of ~0.2 to 2 MT. If only the NATO and Warsaw Pact nations were subject to bombardment, the number of warheads needed to destroy the equivalent of two-thirds of the world refining capacity might be ~0.4 to 4 MT carried by ~400 warheads. Although petroleum is acknowledged to be a prime target of nuclear weapons (*23*), we are not suggesting that it would be an exclusive target.
25. B. S. Haynes and H. Gg. Wagner, *Prog. Energy Combust. Sci.* **7**, 229 (1981). Typical spherules have a density of about 1.9 g/cm$^3$ [A. I. Medalia and L. W. Richards, *J. Colloid Interface Sci.* **40**, 233 (1972)], compared to that of pure graphite, 2.25 g/cm$^3$.
26. G. W. Mulholland, R. D. Mountain, H. Baum, National Bureau of Standards Rep. NBSIR 86-3342 (U.S. Department of Commerce, Washington, DC, 1986).
27. M. V. Berry and I. C. Percival, *Opt. Acta* **33**, 577 (1986).
28. J. Nelson, *Nature* **339**, 611 (1989).
29. R. P. Turco and G. S. Golitsyn, *Environment* **30**, 8 (1988).
30. The nonsoot components efficiently scatter light and thus may also affect climate if large enough quantities are present. Whereas ~10 Tg of pure soot is sufficient to produce a significant global radiative perturbation, ~100 Tg of purely scattering aerosol (for example, dust) might be needed to cause a comparable effect (*2, 3*).
31. A. Tewarson, J. L. Lee, R. F. Pion, "The influence of oxygen concentration on fuel parameters," *18th Symp. (International) on Combustion* (The Combustion Institute, Pittsburgh, PA, 1980), p. 563.
32. G. W. Mulholland, H. Baum, N. Bryner, J. Quintiere, "Smoke emission and optical property measurements at NBS", progress report (National Bureau of Standards, Gaithersburg, MD, 1988).
33. R. L. Dod, N. J. Brown, F. W. Mowrer, T. Novakov, R. B. Williamson, *Aerosol Sci. Tech.* **10**, 20 (1989).
34. G. S. Golitsyn, A. K. Shukurov, A. S. Ginsburg, A. G. Sutugin, A. V. Andronova, *Izv. Atmos. Ocean Phys.* **24**, 227 (1988); A. V. Andronova *et al.*, *ibid.*, p. 235.
35. E. M. Patterson, C. K. McMahon, D. E. Ward, *Geophys. Res. Lett* **13**, 129 (1986).
36. W. Einfeld, B. V. Mokler, B. D. Zak, D. J. Morrison, "A characterization of smoke particles from small, medium, and large-scale hydrocarbon pool fires," M. S. Pilat and E. J. Davis, Eds. (Abstracts of the American Association of Aerosol Research Annual Meeting, Seattle, WA, 14 to 17 September 1987), p. 54. On the basis of these and other measurements, soot-emission factors for petroleum, plastics, asphalt, and other materials obtained in medium-scale laboratory fires appear to be directly applicable to nuclear winter assessments.
37. L. F. Radke, D. A. Hegg, J. H. Lyons, C. A. Brock, P. V. Hobbs, in *Aerosols and Climate*, P. V. Hobbs and M. P. McCormick, Eds. (Deepak, Hampton, VA, 1988), pp. 411–422.
38. By scavenging we specifically mean the incorporation of smoke into water droplets and ice crystals by processes such as nucleation and Brownian diffusion. By removal we specifically mean the purging of scavenged smoke from clouds by precipitation, to the ground, or to low altitudes. Clearly, the removal efficiency is less (in many instances much less) than the scavenging efficiency.
39. W. M. Porch, J. E. Penner, and D. A. Gillette [*Atmos. Env.* **20**, 919 (1986); *ibid.* **21**, 1250 (1987); *ibid.*, p. 2066] propose that soot may be effectively scavenged by windblown dust and ash particles in large fires. However, the mechanism is too inefficient to be of any importance in the general case [R. P. Turco, O. B. Toon, T. P. Ackerman, *Atmos. Env.* **21**, 1247 (1987); *ibid.*, p. 2065].
40. W. R. Cotton, *Am. Sci.* **73**, 275 (1985).
41. H. R. Pruppacher and J. D. Klett, *Microphysics of Clouds and Precipitation* (Reidel, Dordrecht, Holland, 1978).
42. R. J. Charlson and J. A. Ogren, in *Particulate Carbon: Atmospheric Life Cycle*, G. T. Wolff and R. L. Klimisch, Eds. (Plenum, New York, 1982), p. 3.
43. J. Hallett, J. G. Hudson, C. F. Rogers, *Aerosol Sci. Tech.* **10**, 70 (1989). Acetylene soot extracted from a laboratory flue and soot collected from a large pool of burning diesel fuel, when ≤1 hour old, had ≤10% CCN activity at typical cloud supersaturations of ~1%. See also L. F. Radke *et al.*, *Proceedings of the Third World Meteorological Organization Conference on Weather Modification*, Clermont-Ferrand, France, 21 to 25 July 1980 (World Meteorological Organization,

Geneva, 1980).
44. W. H. Benner, A. D. A. Hansen, T. Novakov, *Aerosol Sci. Tech.* **10**, 84 (1989). The fraction of soot scavenged at high supersaturations (>5 to 10%) in a fog chamber ranged from 10 to 95%, with the greatest fractions at the lowest soot concentrations.
45. S. Twomey, *Atmospheric Aerosols* (Elsevier, New York, 1977).
46. R. C. Eagen, P. V. Hobbs, L. F. Radke [*J. Appl. Meteorol.* **13**, 553 (1974)] measured about $6 \times 10^{10}$ CCN per gram of smoke in a forest-fire plume. Hallett *et al.* (*43*) found the smoke produced from vaporized oil quite active as a source of CCN. Such oily smoke particles produced in smoldering combustion, and entrained into large fire plumes, would act as preferential sites for nucleation.
47. J. G. Hudson, *J. Atmos. Sci.* **40**, 480 (1983).
48. F. H. Ludlam, *Clouds and Storms* (Pennsylvania State Univ. Press, University Park, 1980). Intense natural convective systems can have precipitation efficiencies as low as 20%.
49. L. L. Edwards and J. E. Penner, "Potential nucleation scavenging of smoke over large fires: A parametric study," *Lawrence Livermore National Laboratory Rep. UCRL-96242* (Livermore, CA, 1987). Even though soot particles were inappropriately assumed to be spherical and hygroscopic, and suppression of scavenging by ice processes (*40*) was neglected, the predicted scavenging efficiencies were still <60%. Under realistic assumptions, the fraction of fine hydrophobic soot particles removed would be much lower. Using the soot CCN activity measured in (*43*), we estimate ~10% removal for the Edwards and Penner simulation.
50. J. E. Penner and C. R. Molenkamp, *Aerosol Sci. Tech.* **10**, 51 (1989); (*29*).
51. Non-CCN soot particles may, over time, be transformed into active CCN by collecting hygroscopic materials such as sulfates and nitrates or by coagulating with existing CCN. However, significant transformation is not likely to occur in the few minutes it takes the soot to reach the condensation zone in a buoyant fire plume; chemical reactions typically require hours to days, whereas the coagulation of soot particles with CCN at a concentration of $10^5$ CCN per centimeter cubed requires several hours.
52. Whereas the number of particles scavenged may be small, the fractional mass scavenged could be considerably greater if the largest particles are the most active CCN. Larger particles are also more efficiently collected by mechanical processes (*41*). Recent laboratory evidence suggests that larger aggregated soot particles are not significantly more active as CCN (C. F. Rogers, J. Hallett, J. G. Hudson, lecture given at the Air Pollution Control Association Conference, Anaheim, CA, 25 to 30 June 1989).
53. J. E. Penner, L. C. Haselman, Jr., L. L. Edwards, *J. Clim. Appl. Meteorol.* **25**, 1434 (1986).
54. R. D. Small and K. E. Heikes, *J. Appl. Meteorol.*, in press.
55. S. J. Pyne and P. N. Omi, "Wildland fires and nuclear winters," *Defense Nuclear Agency Rep. DNA-TR-85-396* (Washington, DC, 1986).
56. S. L. Thompson and S. H. Schneider, *Foreign Affairs* **65**, 981 (summer 1986).
57. A reasonable estimate of the mass of water injected into the middle troposphere by fire convection is $\sim 10^4$ Tg (that is, ~100 times the mass of smoke); limited surface humidity and precipitation from the convective "cold trap" prevents much larger water injections. Natural convection redistributes $\sim 10^6$ Tg of water per day from the boundary layer, and the total atmospheric mass of water is $\sim 10^7$ Tg.
58. The water vapor partial pressure in a stabilized fire plume at 100 mb would generally be less than about 2 mmHg (that is, equivalent to an initial surface humidity of about 20 mmHg, with no entrainment of drier air as the plume rose). This corresponds to a frost point temperature of −10°C (263 K). Assuming an ambient temperature of −50°C (223 K) at 100 mb, condensed water would dissipate if the air remained undiluted, but warmed by about 40°C, or if the temperature remained fixed, but the humid smoke was diluted with ambient 100-mb air in a ratio of roughly 100:1. Heating and dilution sufficient to dissipate condensation would occur on a time scale of ~1 day (also see the section on dispersion and the references therein).
59. The absorption of light by soot can be represented using an average specific absorptivity (or absorption coefficient), $\sigma_a$ ($m^2$/g-soot). The dimensionless absorption optical depth of a layer of soot is then given by $\tau_a = \sigma_a m_s \ell$, where $\tau_a$ is the absorption optical depth, $m_s$ is the soot mass loading (g/$m^3$) in air, and $\ell$ is the vertical thickness of the soot layer (m). If a total mass of soot is specified, one can estimate $\tau_a = \sigma_a M_s/A$, where $M_s$ is the total soot mass (g) and $A$ is the assumed area of spreading ($m^2$). The absorption optical depth produced by a given mass of fuel burned may be estimated as $\tau_a = \epsilon\sigma_a M_f/A$, where $\epsilon$ is the average soot emission factor (g-soot/g-fuel) and $M_f$ is the fuel mass (g). Occasionally, the specific absorptivity is referenced against the mass of fuel burned; in this case, $\hat{\sigma}_a \equiv \epsilon\sigma_a$ and $\tau_a = \hat{\sigma}_a M_f/A$.For sooty smoke, light scattering is usually less than light absorption: $\sigma_s < \sigma_a$. Extinction is the sum of scattering and absorption ($\sigma_e = \sigma_s + \sigma_a$), and the single-scattering albedo is defined as $\bar{\omega} = \sigma_s/\sigma_e$. Typically, $\bar{\omega}_0$ ~0.1 to 0.4 for soot at visible wavelengths and ~0.75 to 0.95 for vegetation smoke.
60. Such studies include A. D. Clarke, *Appl. Optics* **21**, 3011 (1982); H. Rosen, A. D. A. Hansen, L. Gundel, T. Novakov, *ibid.* **17**, 3859 (1978).
61. D. M. Roessler and F. R. Faxvog, *J. Opt. Soc. Am.* **70**, 230 (1980).
62. K.-T. Lee, thesis, University of Washington (1983).
63. L. Appleby, I. Colbeck, E. Hardman, R. M. Harrison, "Report on research activities at University of Essex to examine 'smoke' optical properties and morphology," Paper MO.10.88, presented at the SCOPE-ENUWAR (Environmental Effects of NUclear WAR) Moscow Workshop, 21 to 25 March 1988. The specific absorptivity of undiluted samples of soot held in a tank for 16 hours decreased by up to 30% from ~9 $m^2$/g to 6 to 7 $m^2$/g.
64. J. Janzen, *Appl. Optics* **19**, 2977 (1980); an equivalent volume sphere was used as the measure of aggregate size.
65. The observed mechanical behavior of aggregates exposed to humidity can be explained by the capillary condensation of vapors within cavities between branches of the aggregate, causing surface tension and capillary pressure to collapse the cluster (R. Turco, P. Hamill, O. Toon, "Capillary nucleation of soot," Third International Conference on Carbonaceous Particles, Berkeley, CA, 5 to 8 October 1987).
66. A. D. Clarke, K. J. Noone, J. Heintzenberg, S. G. Warren, D. S. Covert, *Atmos. Env.* **21**, 1455 (1987); *Appl. Optics* **21**, 370 (1982).
67. T. P. Ackerman and O. B. Toon, *Appl. Optics* **20**, 3661 (1981).
68. R. F. Pueschel *et al.*, *J. Geophys. Res.* **93**, 8388 (1988).
69. This is caused in part by the dependence of absorption and scattering on wavelength ($\lambda$) in the Rayleigh limit (that is, for particle sizes $<<\lambda$), in which the absorption varies as $\lambda^{-1}$ and the scattering as $\lambda^{-4}$. At visible and infrared wavelengths, soot aggregates apparently follow the Rayleigh law of absorption for a variety of morphologies (*27, 28*).
70. C. W. Bruce and N. M. Richardson, *Appl. Optics* **22**, 1051 (1983).
71. Other data are generally consistent with this conclusion [E. E. Uthe, B. M. Morley, N. B. Nielsen, *Appl. Optics* **21**, 460 (1982); E. F. O'Sullivan and B. K. Ghosh, in *Combustion Institute European Symposium 1973*, F. J. Weinberg, Ed. (Academic Press, New York, 1973), p. 195].
72. P. P. Anikin and A. K. Shukurov, *Izv. Atmos. Ocean Phys.* **24**, 247 (1988); I. N. Sokolik, *ibid.*, p. 274.
73. We have calculated the influence of coagulation on smoke optical properties using a multicomponent, size-resolved aerosol model that accounts for both vertical and horizontal dispersion (*2*). In the model, "equivalent spherical" particles were assumed in determining the evolution of physical and optical properties. On this basis, the smoke absorption decreased by a factor of ~2 over 1 month (with most of the decrease occurring in the first week) for reasonable plume dispersion rates. Because the spherical approximation significantly underestimates the absorptivity of the soot component, the actual decrease might be only ~20 to 30%—a second-order effect.
74. V. R. Deitz and J. L. Bitner, *Carbon* **11**, 393 (1983); W. D. Ellis and P. V. Tometz, *Atmos. Env.* **6**, 707 (1972). Elemental carbon also reacts significantly with OH and O [(M. F. R. Mulcahy and B. C. Young, *Carbon* **13**, 115 (1975)].
75. S. L. Stephens, J. G. Calvert, J. W. Birks, *Aerosol Sci. Tech.* **10**, 326 (1989); S. L. Stephens, M. J. Rossi, D. M. Golden, *Int. J. Chem. Kinetics* **18**, 1133 (1986).
76. J. A. Ogren, in *Particulate Carbon: Atmospheric Life Cycle*, G. T. Wolff and R. L. Klimisch, Eds. (Plenum, New York, 1982), p. 379. The washout lifetime of background soot has been estimated to be between about 2 days and 1 month, depending on meteorological conditions [J. A. Ogren and R. J. Charlson, *Tellus* **35B**, 241 (1983)].
77. L. A. Barrie, *J. Geophys. Res.* **90**, 5789 (1985).
78. J. Heintzenberg, *Atmos. Env.* **16**, 2461 (1982).
79. R. Dlugi, *Aerosol. Sci. Tech.* **10**, 93 (1989).
80. B. W. Golding, P. Goldsmith, N. A. Machin, A. Slingo, *Nature* **319**, 301 (1986).
81. D. L. Westphal, O. B. Toon, W. R. McKie, in preparation; D. L. Westphal, O. B. Toon, T. N. Carlson, *J. Atmos. Sci.* **45**, 2145 (1988).
82. F. Giorgi, *J. Geophys. Res.* **94**, 1127 (1989); F. Giorgi and G. Visconti, *ibid.*, p. 1145.
83. A. Robock, *Science* **242**, 911 (1988); in *Aerosols and Climate*, P. V. Hobbs and M. P. McCormick, Eds. (Deepak, Hampton, VA, 1988).
84. The efficient mesoscale dispersion of particulate clouds is readily seen in satellite images of wildfire plumes [Y.-S. Chung and H. V. Le, *Atmos. Env.* **18**, 2143 (1984); R. S. Fraser, Y. J. Kaufman, R. L. Mahoney, *ibid.*, p. 2577].
85. N. N. Veltishchev, A. S. Ginsburg, G. S. Golitsyn, *Izv. Atmos. Ocean Phys.* **24**, 296 (1988).
86. H. Wexler [*Weatherwise* **3**, 129 (1950)] reported that the smoke cloud from the Alberta, Canada, forest fire of 1950 lowered surface temperatures in Washington, DC, by 4° to 6°C.
87. V. Ramaswamy and J. T. Kiehl, *J. Geophys. Res.* **90**, 5597 (1985); other workers have made similar radiative energy balance calculations [G. S. Golitsyn and A. S. Ginsburg, *Tellus* **37B**, 173 (1985)].
88. G. S. Golitsyn and A. K. Shukurov, *Doklady USSR Acad. Sci.* **297**, 1334 (1987). An analysis of some 50 dust storms in Tadjikistan, U.S.S.R., showed that daytime surface temperatures were depressed by as much as 10° to 12°C.
89. The nuclear dust problem was initially considered in (*2*) and was more fully developed in (*3*) and (*4*). Although soil dust has a low absorption coefficient (≤0.1 $m^2$/g), its scattering properties could be important in scenarios based on "counterforce" targeting.
90. R. M. Haberle, T. P. Ackerman, O. B. Toon, J. L. Hollingsworth, *Geophys. Res. Lett.* **12**, 405 (1985).
91. J. Kirkwood, J. Sanborn, R. Turco, "Contribution of model parameter uncertainties to uncertainties in the TTAPS analysis of Nuclear Winter," *Report 130000-5* (R&D Associates, Los Angeles, CA, 1984).
92. The average reduction factor for solar insolation, disregarding the effect of scattering, may be estimated as $\exp(-\mu\tau_a)$, where $\mu \cong \sqrt{3}$ is an average solar zenith angle factor.
93. The three SCOPE scenarios correspond to soot absorption optical depths of 0.3, 1.0, and 3.0; in each case, a unique vertical injection profile for the soot is defined. Optical properties, season of injection, and other parameters are also specified (*8*).
94. The infrared opacity of smoke can trap upwelling surface heat radiation in the atmospheric window (8 to 13 μm) and can increase the emissivity of the upper air layers heated by solar absorption, thus allowing more thermal energy to be emitted to the ground (which is partly offset by more efficient cooling of the heated layers through emission to space).
95. F. P. J. Valero, T. P. Ackerman, W. J. Y. Gore, *Geophys. Res. Lett.* **10**, 1184 (1983).
96. S. G. Warren and W. J. Wiscombe, *Nature* **313**, 467 (1985).
97. T. S. Ledley and S. L. Thompson, *Clim. Change* **8**, 155 (1986).
98. A. M. Vogelman, A. Robock, R. G. Ellingson, *J. Geophys. Res.* **93**, 5319 (1988).

99. M. C. MacCracken, "Nuclear war: Preliminary estimates of the climatic effects of a nuclear exchange," *Lawrence Livermore National Laboratory Report UCRL-89770* (Livermore, CA, 1983).
100. V. V. Aleksandrov and G. L. Stenchikov, "On the modeling of the climatic consequences of the nuclear war," *Computing Center of the Academy of Sciences of the USSR* (Moscow, 1983).
101. C. Covey, S. H. Schneider, S. L. Thompson, *Nature* **308**, 21 (1984).
102. M. C. MacCracken and J. J. Walton, "The effects of interactive transport and scavenging of smoke on the calculated temperature change resulting from large amounts of smoke," *Lawrence Livermore National Laboratory Report UCRL-91446*, (Livermore, CA, 1984).
103. A. Robock, *Nature* **310**, 667 (1984).
104. S. L. Thompson, *ibid.* **317**, 35 (1985).
105. R. C. Malone, L. H. Auer, G. A. Glatzmaier, M. C. Wood, O. B. Toon, *Science* **230**, 317 (1985); *J. Geophys. Res.* **91**, 1039 (1986).
106. C. Covey, S. L. Thompson, S. H. Schneider, *J. Geophys. Res.* **90**, 5615 (1985).
107. R. D. Cess, G. L. Potter, S. J. Ghan, W. L. Gates, *ibid.*, p. 12937.
108. G. L. Stenchikov and P. Carl, "Climatic consequences of nuclear war: Sensitivity against large-scale inhomogeneities in the initial atmospheric pollutions" (Central Inst. Electron Physics, Berlin, German Democratic Republic, 1985).
109. C. Covey, *BioScience* **35**, 563 (1985).
110. R. K. R. Vupputuri, *Atmos. Env.* **20**, 665 (1986).
111. C. Covey, *Nature* **325**, 701 (1987).
112. S. L. Thompson, V. Ramaswamy, C. Covey, *J. Geophys. Res.* **92**, 10942 (1987).
113. J. F. B. Mitchell and A. Slingo, *ibid.* **93**, 7037 (1988).
114. S. J. Ghan, M. C. MacCracken, J. J. Walton, *ibid.*, p. 8315.
115. G. A. Glatzmaier and R. C. Malone, "Global climate simulations of the ENUWAR case studies," paper MO.16.88, presented at the SCOPE-ENUWAR Moscow Workshop, 21 to 25 March 1988.
116. G. Stenchikov and P. Carl, "First acute phase stress matrix calculations using the CCAS tropospheric general circulation model," paper MO.26.88, presented at the SCOPE-ENUWAR Moscow Workshop, 21 to 25 March 1988.
117. A. B. Pittock, J. S. Frederiksen, J. R. Garratt, K. Walsh, in *Aerosols and Climate*, P. V. Hobbs and M. P. McCormick, Eds. (Deepak, Hampton, VA, 1988), pp. 395–410.
118. R. M. Haberle, *Science* **234**, 459 (1986). In this case, planetwide Martian dust storms provide an analog for aerosol heating by solar absorption, leading to self-lofting and accelerated global dispersion.
119. T. P. Ackerman, R. P. Turco, O. B. Toon, in *Aerosols and Climate*, P. V. Hobbs and M. P. McCormick, Eds. (Deepak, Hampton, VA, 1988), pp. 443–458.
120. A. B. Pittock, K. Walsh, J. S. Frederiksen, *Clim. Dyn.* **1**, 191 (1989).
121. Interactive climate feedback predictions involve, among other things, representations of sea ice, snow cover, cloud albedo, and sea-surface temperature. Current model parameterizations for these physical elements are not thought to be reliable over long times in perturbed states.
122. T. R. Mettlach *et al.*, *J. Geophys. Res.* **92**, 1967 (1987).
123. R. Malone and G. Glatzmaier, paper presented at SCOPE-ENUWAR Moscow Workshop, 21 to 25 March 1988; S. Thompson and P. Crutzen, paper presented at DNA Global Effects Meeting, Santa Barbara, CA, 19 to 21 April 1988. Both groups discussed preliminary three-dimensional model calculations of ozone transport and photochemistry in a nuclear winter–perturbed atmosphere. Earlier studies had considered the effects on ozone of the $NO_x$ chemistry and smoke heating (*110*), but not the redistribution of ozone by anomalous large-scale dynamics.
124. D. Lubin, J. E. Frederick, A. J. Krueger, *J. Geophys. Res.* **94**, 8491 (1989).
125. National Research Council, *Causes and Effects of Changes in Stratospheric Ozone: Update 1983* (National Academy Press, Washington, DC, 1984).
126. These "scenario" uncertainties are "irreducible" in the sense that they involve imprecisely known factors including: the circumstances that might instigate the use of nuclear weapons; the course of escalation; the aggregate number of weapons used; the specific targets, heights, and yields of burst; weapons performance; ignition probability at target sites; and details of the impinging meteorology. Nonetheless, with the existing and projected (near-term) nuclear forces (*21*), the sequence of events leading to a nuclear exchange is clearly possible (*4*), and the likelihood of massive smoke emissions in that circumstance is high (*14*).
127. R. P. Turco, *Ambio* **18**, 391 (1989).
128. J. W. Birks and S. L. Stephens, in (*12*), pp. 155–166; S. L. Stephens and J. W. Birks, *BioScience* **35**, 557 (1985).
129. D. A. Hegg *et al.*, *J. Geophys. Res.* **92**, 14701 (1988).
130. For example, in the original TTAPS study the total flammable burden was overestimated by a factor of 2 to 3, the soot emission factor was underestimated by a factor of ~5, the soot prompt scavenging was overestimated by a factor of ~2, and the soot visible absorptivity (per unit mass) was roughly correct. Overall, the derived optical depths were comparable to current values (*8*).
131. *International Petroleum Encyclopedia* (Penn Well, Tulsa, OK, 1986).
132. Office of Technology Assessment, "The Effects of Nuclear War," Washington, DC, 1979.
133. S. Glasstone and P. J. Dolan, *Effects of Nuclear Weapons* (Department of Defense, Washington, DC, 1977).
134. For valuable discussions and advice, we thank E. Anders, D. Auton, D. Bacon, J. Birks, T. Bunch, R. Chuan, A. Clarke, W. Cotton, W. Cropper, P. Crutzen, D. Fields, S. Ghan, G. Glatzmaier, G. Golitsyn, H. Grover, R. Haberle, J. Hallett, R. Harrison, M. Harwell, P. Hobbs, J. Hudson, M. MacCracken, R. Malone, S. Marcus, J. Mitchell, G. Mulholland, E. Patterson, J. Penner, I. Percival, A. B. Pittock, R. Pueschel, L. Radke, A. Robock, F. Rogers, B. Stocks, S. Schneider, D. Silver, R. Small, G. Stenchikov, S. Stephens, S. Thompson, G. Tripoli, D. Ward, D. Westphal, R. B. Williamson, and B. Zak. The work of O.B.T. and J.B.P. was supported by the Defense Nuclear Agency Global Effects Program managed by D. Auton through Interagency Cost Reimbursible Order 88-880.

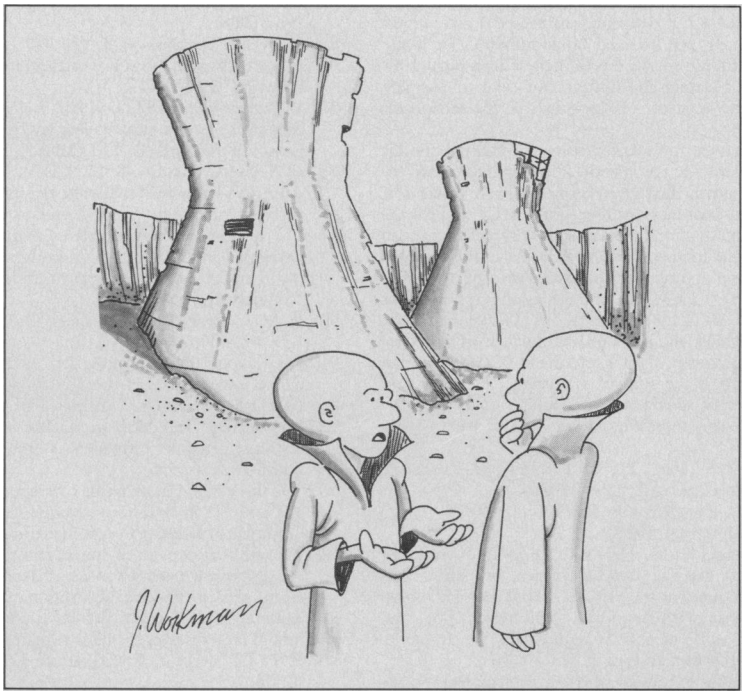


***"As you can see we've unearthed another one. If we ever find one that was completed maybe we'll understand what they were for."***